Encapsulation of heavy metals by a nanoporous complex oxide $12CaO•7Al_2O_3$

Navaratnarajah Kuganathan[1,a)], Robin W Grimes[1] and Alexander Chroneos[1,2,b)]

[1]Department of Materials, Imperial College London, London, SW7 2AZ, United Kingdom

[2]Faculty of Engineering, Environment and Computing, Coventry University, Priory Street, Coventry CV1 5FB, United Kingdom

Abstract

The nanoporous oxide $12CaO•7Al_2O_3$ (C12A7) offers the possibility of capturing large concentrations of environmentally damaging extra-framework species in its nanopores. Using density functional theory with a dispersion correction (DFT+D), we predict the structures and energetics of some heavy metals (Cr, Ni, Cu, Zn, Cd, Hg and Pb) trapped by the stoichiometric and electride form of C12A7. In the stoichiometric form, while Zn, Cd, Hg and Pb are encapsulated weakly, Cr, Ni and Cu exhibit strong encapsulation energies. The electride form of C12A7 shows a significant enhancement in the encapsulation of Cr, Ni, Cu and Pb. Successive encapsulation of multiple Cr, Ni, Cu and Pb as single species in adjacent cages of C12A7 is also energetically favourable.

[1]Corresponding authors, e-mails: a) n.kuganathan@imperial.ac.uk ; b) alexander.chroneos@imperial.ac.uk

This manuscript was accepted by J. Appl. Phys. Click here to see the version of record.

1. Introduction

Substantial volumes of toxic heavy metals such as Cd, Pb, Cu, Zn and Cr are produced as a by-product of rapid industrial activity including electroplating, smelting, mining operations and battery manufacturing[1-7]. As heavy metals cannot be degraded or destroyed, there is potential damage to the environment and humans when acceptable levels are exceeded. This is because heavy metals damage human physiology directly or indirectly. For example, increased levels of nickel can cause kidney and lung disease[8]; lead damages central nervous system, the kidney, liver and reproductive system[9]; cadmium has been identified by the US Environmental agency as a probable human carcinogen[10]. Consequently, there is a necessity to reduce the level of toxic heavy metals in the environment.

Many technologies such as ion-exchange, solvent extraction, coagulation and adsorption have been used to remove heavy metals[11-15]. Significant effort has been devoted to remove heavy metals from polluted water by adsorption as it is an efficient and economical method[16]. A variety of sorbents such as activated carbon, carbon nanotubes, synthetic oxides and zeolites have been studied extensively[17-20]. Porous materials are promising candidates as they exhibit a high capacity to incorporate heavy metals[21-24].

The nanoporous complex inorganic oxide $12CaO{\bullet}7Al_2O_3$ (C12A7) is a candidate material to incorporate large concentration of heavy metals as it provides 12 subnanometer cages per unit cell[25-27]. In addition, it exhibits high chemical and thermal stability[27]. Its constituent metal oxides (Al_2O_3 and CaO), are highly abundant and non-toxic. The framework of C12A7 is represented using the chemical formula $[Ca_{24}Al_{28}O_{64}]^{4+}$, that is, every cage bears a charge of $+\frac{1}{3}$. The positive charge of the framework is compensated by negative ions occupying some of the cages [e.g. two O^{2-} ions in stoichiometric C12A7 ($C12A7{:}O^{2-}$)[25,26], four OH^- ions in fully hydrated C12A7[28,29], and four electrons in the electride form of C12A7 ($C12A7{:}e^-$)][30,31]. The extraframework O^{2-} ions in stoichiometric C12A7 are relatively loosely bound to the framework and can be either removed or replaced with species such as H^-,[29] Au^-,[32] and O_2.[2-33]

In the present study, we use density functional theory (DFT) together with dispersion corrections (DFT+D) to investigate the thermodynamical stability of encapsulating gaseous heavy metals (Cr, Ni, Cu, Zn, Cd, Hg and Pb) that are present in the form of gaseous atoms in air as air pollutants within both the stoichiometric and electride forms of C12A7. DFT calculations, in addition to structural information, predict electronic structure and property values.

2. Computational Methods

This manuscript was accepted by J. Appl. Phys. Click here to see the version of record.

All calculations were carried out using the spin-polarized mode of DFT as implemented in the VASP[34,35] package. The exchange-correlation term was modelled using the generalized gradient approximation (GGA) parameterized by Perdew, Burke, and Ernzerhof (PBE)[36]. The C12A7 lattice is cubic with the lattice constant of 11.99 Å. Stoichiometric and electride forms of supercell contained 118 and 116 atoms respectively. In all cases, we have used a plane-wave basis set with a cut-off value of 500 eV and a 2×2×2 Monkhorst-Pack[37]k-point mesh, which yields 8 k-points. Further increase in the k-points resulted in a total energy difference of only 0.6 meV per atom. The density of plots (DOSs) were plotted using a 4×4×4 Monkhorst-Pack k-point mesh. Structural optimisations were performed using a conjugate gradient algorithm[38] and the forces on the atoms were obtained via the Hellman-Feynmann theorem, including Pulay corrections. In all optimized structures, forces on the atoms were smaller than 0.001 eV/Å and all the values in the atomic stress tensor were less than 0.002 GPa. We define the normalised encapsulation energy per atom to encapsulate n number of heavy metal atoms inside empty cages of the electride form of C12A7 through the following equation:

$$E_{Enc} = [E(nHM\text{-}C12A7{:}e^-) - E(C12A7{:}e^-) - n\,E(HM)]/n \quad (1)$$

where E (C12A7:e⁻) is the total energy for bulk C12A7:e⁻, E (nHM-C12A7:e⁻) is the total energy of n number of heavy metal atom occupying the cages, E(HM) is the total energy of an isolated heavy metal atom (the reference state) and n is the number of heavy metal atoms considered in the process.

The inclusion of van der Waals (vdW) interactions is particularly important for the incorporation of highly polarizable heavy metal atoms. Here, semi-empirical dispersion correction has been included as implemented by Grimme *et al.*[39] [DFT-D3 (zero)] in VASP. Since the results of the calculations depend on whether are carried out at isobaric (P=const) or at isochoric (V=const) conditions[40]- for example, the energy depends on pressure, e.g., see reference 41- we clarify that all calculations have been performed here at isobaric conditions thus no further thermodynamical corrections are needed.

3. Results

3.1. Structural modelling of C12A7:O^{2-} and C12A7:e^-.

C12A7 exhibits a cubic crystallographic structure with space group $I\bar{4}3d$ and lattice constant of 11.99 Å[26]. The unit cell is composed of two $12CaO{\bullet}7Al_2O_3$ molecules (118 atoms) with twelve cages. Each empty cage has an inner free space of approximately 4 Å radius and contains 16 O ions, 8 Al ions and 6 Ca ions. The chemical composition of the unit cell can be expressed as $[Ca_{24}Al_{28}O_{64}]^{4+}{\bullet}(O^{2-})_2$, where $[Ca_{24}Al_{28}O_{64}]^{4+}$ is a positively

charged framework (see Figure 1a) with two extra-framework oxide ions occupying two of the cages (see Figure 1b). The electride form of C12A7 $[Ca_{24}Al_{28}O_{64}]^{4+}\bullet(e^-)_4]$ replaces the two extra-framework oxygen ions by four electrons; the four electrons are localized in twelve equivalent cages with the average occupation number of $\frac{1}{3}$ electrons per cage.

The starting point of the present study was to reproduce the experimental structure of C12A7:O^{2-} to enable an assessment of the quality and efficacy of the pseudopotentials and basis set used in this study. The calculated equilibrium lattice parameters (a=12.04 Å, b=c=12.01 Å, α=90.02°, β=89.95° and γ=89.93°) are in excellent agreement with experimental lattice parameters (a=b=c=11.99 Å and α=β= γ=90.0°)[26]. In the relaxed structure of stoichiometric C12A7, the extra-framework O^{2-} ion occupies an "off-centre" site. This is due to the strong perturbation between the extra-framework O^{2-} ion and the cage wall (see Figure 1b). This perturbation introduces a small distortion in the calculated lattice parameters. In the real material the extra-framework O^{2-} are disordered across the material leading to an average cubic symmetry; in the simulation an ordering is imposed. Nevertheless, the distortion from cubic symmetry is so small that this is an acceptable approximation. The calculated equilibrium lattice parameters for C12A7:e^- were a=b=c=12.06 Å and α=β= γ=90.0°. Thus, the lattice volume of C12A7: e^- is only slightly greater than that of C12A7:O^{2-}.

3.2. Electronic properties of C12A7:O^{2-} and C12A7:e^-

In this section, we briefly describe the electronic structures of the stoichiometric and electride forms of C12A7. The calculated DOS for C12A7:O^{2-} is shown in Figure 2a and is consistent with C12A7:O^{2-} being an insulator. The top of the valence band, formed by the *2p* states of framework oxide ions, is at approximately 1.3 eV, agreeing well with the previous theoretical study[42]. The two peaks at 2.8 eV correspond to the *2p* states of extra-framework oxide ions. The lower energy peak corresponds to the *2p* states interacting with two Ca^{2+} ions (i.e. bonding) and the higher energy peak is due to the *2p* states perpendicular to the bonding direction (i.e. non-bonded). The partial distribution of the charge density associated with two extra-framework oxide ions localised within the cages is shown in Figure 2c.

Figure 2b shows the calculated DOS for C12A7:e^-. The localised extra-framework electrons within the cages results in the system being metallic. The partial distribution of the charge density associated with the extra-framework localised electrons is shown in Figure 2d. The

This manuscript was accepted by J. Appl. Phys. Click here to see the version of record.

four electrons in a cubic unit cell are uniformly distributed to form twelve ellipsoid like iso-surfaces (with an average of $\frac{1}{3}$ electrons per cage).

3.3. Encapsulation of single heavy metal atoms in a cage of C12A7:O^{2-}

A single metal atom was incorporated into one of the ten empty cages in stoichiometic C12A7 to investigate the stability of heavy metals inside C12A7:O^{2-}. The relaxed structures of the cage containing different metals atom are shown in Figure 3. Encapsulation energies calculated using a single atom reference state, and the Bader charge on metal atoms, are reported in Table 1. There are different charge analysis methods such as the Hirshfeld charge analysis[43] available. In many cases, sum of the calculated partial atomic Bader charges of molecules are not equal to the total charge of the molecule. At any rate, some methods work better than others. Nevertheless, the particular analysis throughout the system would provide the right trend. The degree of interaction between the heavy metals and cage wall ions are dipicted in Table 2 in terms of bond distances.

Zn, Cd and Hg occupy the centre of the cage, forming weak bonds with cage wall Ca^{2+} ions and no significant bonds with Al^{3+} or O^{2-} ions. This is reflected in the very low negative encapsulation energies (mainly due to the van der Waals interaction) and small Bader charge (refer to Table 1). As the valence electronic configuration ($d^{10}s^2$) of these three metals is complete and stable, they prefer to maintain their unaltered valence electronic configurations. The slightly more favourable encapsulation energy for Zn is due to its smaller size compared to Cd and Hg. Encapsulation of these three metals distorts the Ca-Ca cross cage distance (from 5.66 Å) as defined in Figure 3. The smaller distortion for Zn (see Table 2) is due to its smaller size.

Pb exhibits a weak encapsulation energy commensurate with its smaller Bader charge. This is due to the weak interaction between Pb and O in the cage wall (see Figure 3). The larger size of Pb introduces the larger distortion in the Ca-Ca cage pole.

Nickel is strongly trapped exhibiting an encapsulation energy of −1.70 eV. This is because of the strong interaction of Ni with O and Ca ions (refer to bond distances in Table 2) as evidenced by the slightly off-centred position of Ni in the relaxed structure. The reactivity of Ni with the cage wall is due to its open-shell valence electronic configuration (d^8s^2). The very small Bader charge on Ni (+0.02) is due to the balance of its interaction with cations and anions.

The negative encapsulation energy for Cr (−1.53 eV) reveals that it is more stable inside the cage than as an isolated atom. As with Ni there is a slight displacement of Cr towards the cage wall with Cr-O bond formation as evidenced by the Bader charge on Cr (+0.24).

The encapsulation energy for copper is also negative (−1.20 eV), again reflecting the greater bonding afforded by the incomplete valence electronic configuration of Cu ($d^{10}s^{1}$). The energy is, however, not quite as favourable as for Ni and Cr and this is reflected in the almost zero Bader charge. Nevertheless strong Cu-O interactions give rise to the short bond distances reported in Table 2.

Next we considered up to 3 metal atoms (Cr, Ni and Cu) occupying separate adjacent cages (i.e. two of the ten initially empty cages contain a single metal atom and then three of the ten cages contain a metal atom). Figure 4 depicts relaxed adjacent cages each containing single metal atoms.

Calculations reveal that the encapsulation energies of the second atom (M:MC12A7:O^{2-}) and the third atom (M:2MC12A7:O^{2-}) are negative in all cases (see Table 3). The second and third atom incorporation energies for Cr are less negative than the first incorporation energy (refer to Table 3). Conversely, the second and third Ni and Cu atoms incorporate more favourably than the first. This is in part due to the charge distribution among multiple atoms encapsulated.

The net charge of C12A7:O^{2-} crystal structure is zero as it is the stoichiometric form of C12A7. The Bader charges on the Ni and Cu atoms in C12A7:O^{2-} are almost zero. This indicates that both Ni and Cu atoms prefer to be neutral. The encapsulation energies for the second Ni and Cu atoms are −2.57 eV and −2.70 eV respectively and these values are highly negative compared to the respective first encapsulation energy values. According to the Bader charge analysis it is clear that net charge on two Ni or two Cu atoms is almost zero and atoms become polarised (Cu: +0.51, −0.57 Ni: +0.26, −0.26) with equal opposite charge distribution. The degree of polarisation in Cu is greater than in Ni. This polarisation makes the lattice more stable. Thus, the second atom encapsulation is more favoured compared to its first encapsulation giving more negative encapsulation energy. There is a decrease in the third encapsulation for both Cu and Ni. The Bader charge analysis shows that the net charge on two Cu or three Ni is zero. In both cases, charges on the two atoms are almost as those observed in the case of two atoms. But the third atom almost prefers to be neutral. Thus the encapsulation energy of third atom is lower than the second encapsulation energy.

In the case of Cr, the situation is different due to its charges on Cr atoms being different than those on Cu or Ni in the encapsulated structures. The encapsulation energy for the first Cr is −1.53 eV and Cr forms a +0.27 charge. Once the second Cr is encapsulated, the net charge on two Cr atoms is expected to be +0.54. This is achieved by one Cr atom forming +0.81 and the other one forming −0.26. This unequal distribution of charges makes

the system less stable. Therefore, the second encapsulation energy is lower than compared to its first encapsulation energy. The third encapsulation energy of Cr then becomes more negative compared to the second encapsulation energy. This is due to the three Cr atoms almost hold the same amount of positive charges as a single Cr atom does in the case of first encapsulation.

3.4. Encapsulation of single metal atoms in C12A7:e^-

The relaxed configurations of single heavy metal atoms occupying a cage in C12A7:e^- are shown in Figure 5. All the atoms occupy positions close to the centre of the cage (between two Ca ions in the cage wall). Encapsulation energies and Bader charges on metal atoms are reported in Table 4. To compare the deformation of the occupied cage with the unoccupied cage, Ca-Ca distances (as defined in Figure 5) for relaxed structures are reported in Table 5; the distance in the unoccupied cage is 5.70 Å.

The electride form of C12A7 encapsulates all metal atoms more favourably than the stoichiometric form. Significant enhancement in the energy is predicted for Cr, Ni, Cu and Pb. Notably, in all cases there is no significant interaction between cage wall ions (Al^{3+} or O^{2-}) except the two Ca^{2+} ions at the cage poles. This is due to the electron transfer which enables the metals to occupy the centre of the cage and to from an attractive interaction with those two Ca^{2+} ions.

Zn, Cd and Hg exhibit the lowest encapsulation energies in C12A7:e^- due to their complete valence electronic configuration. They are only able to accommodate a very small change ($\leq$ –0.20 |e|) (see Table 4). This is further supported by the longer Ca-Ca distances as reported in Table 5. As a consequence all three atoms exhibit only a weak electrostatic attraction with cage pole Ca^{2+} ions.

Ni exhibits a particularly high encapsulation energy (see Table 4). This is reflected in the shortest Ca-Ca and Ni-Ca distances (see Table 5) but also the largest (negative) Bader charge. The charge on Ni is commensurate with part filling its open d-shell, which is short of two electrons.

The second most negative encapsulation energy is predicted for Cu (see Table 4). Again charge can be accommodated in the partly occupied valance orbitals, Cu ($d^{10}s^1$) to form the stable Cu^- ($d^{10}s^2$) ion. This is reflected in the Bader charge analysis; approximately –0.60 |e| is gained by the Cu.

There is also a strong driving energy for Pb encapsulation, again mediated by the accommodation of charge from the C12A7:e^- host lattice. The Bader charge analysis shows that 1.30 electrons are transferred to Pb. Since the valence electronic configuration of Pb is

This manuscript was accepted by J. Appl. Phys. Click here to see the version of record.

s^2p^2, the final configuration of Pb after electron transfer is approaching s^2p^4. While still an open shell configuration, further electron transfer is not observed, presumably because of electron repulsion.

Encapsulation energy of Cr is −1.94 eV. The amount of charge transferred to Cr is only −0.33 |e|. This is due to the stable valence electronic configuration of Cr (d^5s^1). Bader charge analysis on Cr indicates that in C12A7:e^-, Cr retains almost its valence electronic configuration. Thus, there is no significant increase in the charge and encapsulation energy compared to the values calculated in C12A7:O^{2-}. Also, we note that the electron affinity of Cr (0.666) is lower than that of Ni (1.156) and Cu (1.228)[44] supporting further to this he present observation.

Successive encapsulation was considered for up to 5 atoms of Cr, Ni, Cu and Pb inside separate unoccupied cages of C12A7:e^-. In the case of Cu, four atoms can be accommodated with almost no change in favourable encapsulation energy. This reflects the four conduction electrons available in the repeat unit lattice. The Bader analysis shows that each Cu gains similar charge up to four successive atoms. As the valence electronic configuration of Cu is $d^{10}s^1$, this reflects that each Cu atom is completing its valence shell to form stable $d^{10}s^2$ configuration. While the fifth copper atom also attracts only slightly less charge, there is a significant reduction in the encapsulation energy. This is because there are no more free electrons left. However, the five Cu atoms share equally almost the same total amount of Bader charge that is gained by four Cu atoms. As a consequence, with the 4th Cu atom, there is a significant Fermi level shift to the top of the valence band for the encapsulation of four Cu atoms and the system becomes insulating (see Figure 6a). This is further illustrated in Figure 6b, which shows how the charge density localisation within the unit cell changes with the addition of 1, 2, 3 and 4 Cu atoms. In 4CuC12A7:e^- almost all electrons have been trapped by the 4 Cu atoms.

Cr maintains almost the same favourable encapsulation energy for successive atoms up to 4 (see Table 6). The Bader charge analysis shows that each atom attracts a similar charge. There is a reduction in the encapsulation energy for the fifth Cr atom and the Bader charge is also reduced by −0.10|e| on each Cr atom (i.e. the total charge hardly changes but it is now distributed on 5 rather than 4 Cr atoms).

For Ni, the encapsulation energy and the Bader charge for the second atom are almost the same as calculated for the first (see Table 6), however, the energy decreases with further encapsulation. This is accompanied by successively lower charge transfer to individual Ni atoms. Bader analysis shows that almost the same total amount of charge, ~2 |e|, is gained

by two, three, four or five encapsulated Ni atoms.

For Pb, there is a reduction in the encapsulation energy for the second incorporation and then for further additions. This is accompanied by a reduction in the charge on each Pb atom. In fact, the sum of the Bader charges on Pb atoms remains roughly constant at −1.5 electrons (see Table 6).

We predict that the encapsulation process should take place *via* the surface of the C12A7. This will also involve kinetic barrier of encapsulation. The complexity of the structure of C12A7 lattice and the lack of experimental data available on the surface structure, constitutes the modelling of surface structures very difficult for both stoichiometric and the electride form of C12A7. One of the barriers to model makes C12A7 surfaces is that this complex structure has no obvious cleavage planes. The distances between atomic planes in C12A7 are much smaller and do not exceed approximately 0.5Å for any combination of the Miller indices. In future work, we will make reasonable model structures for surfaces of both stoichiometric and electride forms of C12A7.

4. Conclusion

DFT+D simulations have been employed to study the capacity of C12A7 to encapsulate key environmentally toxic heavy metals. Both the stoichiometric C12A7:O^{2-} and C12A7:e^{-} forms were studied. While Zn, Cd, Hg and Pb show weak encapsulation in C12A7:O^{2-}, Cr, Ni and Cu exhibit strong encapsulation. Successive encapsulation of Cr, Ni and Cu was considered so that multiple cages within a unit cell are occupied by single atom species. While successive encapsulation is energetically favourable, the encapsulation energy of successive atoms decreases gradually with further additions. C12A7:e^{-} shows a significant enhancement in encapsulation energies over C12A7:O^{2-} due to the availability of extra-framework electrons. Zn, Cd and Hg show weak encapsulation due to their complete valence electronic configurations. Cr, Ni, Cu and Pb show strong encapsulation by accommodating extra-framework electrons in the open-shell electronic configurations that these atoms exhibit. Successive encapsulation is also energetically favourable, but the degree to which additional species will be stable, and hence the loading that might be attained is dependent on the specific valence electronic configuration. In this context Cr shows particular promise.

Conflicts of interest

The authors declare that there is no competing financial interest.

Acknowledgements

We thank the EPSRC for funding as part of the "PACIFIC" programme (grant code

EP/L018616/1). Computational facilities and support were provided by High Performance Computing Centre at Imperial College London.

References

1 X. Wei, X. Kong, S. Wang, H. Xiang, J. Wang and J. Chen, Industrial & Engineering Chemistry Research, 2013, 52, 17583-17590.

2 P. Kapusta and Ł. Sobczyk, Science of The Total Environment, 2015, 536, 517-526.

3 J. Maskall, K. Whitehead and I. Thornton, Environmental Geochemistry and Health, 1995, 17, 127-138.

4 Z. Li, Z. Ma, T. J. van der Kuijp, Z. Yuan and L. Huang, Science of The Total Environment, 2014, 468-469, 843-853.

5 A. P. Puga, L. C. A. Melo, C. A. de Abreu, A. R. Coscione and J. Paz-Ferreiro, Soil and Tillage Research, 2016, 164, 25-33.

6 S. Cao, X. Duan, X. Zhao, B. Wang, J. Ma, D. Fan, C. Sun, B. He, F. Wei and G. Jiang, Environmental Pollution, 2015, 200, 16-23.

7 G. Liu, Y. Yu, J. Hou, W. Xue, X. Liu, Y. Liu, W. Wang, A. Alsaedi, T. Hayat and Z. Liu, Ecological Indicators, 2014, 47, 210-218.

8 C. E. Borba, R. Guirardello, E. A. Silva, M. T. Veit and C. R. G. Tavares, Biochemical Engineering Journal, 2006, 30, 184-191.

9 R. Naseem and S. S. Tahir, Water Research, 2001, 35, 3982-3986.

10 Environmental Protection Agency. Cadmium. Washington (DC): Environmental Protection Agency; 1987

11 F. Fu and Q. Wang, Journal of Environmental Management, 2011, 92, 407-418.

12 A. Dąbrowski, Z. Hubicki, P. Podkościelny and E. Robens, Chemosphere, 2004, 56, 91-106.

13 M. Černá, Environmental Monitoring and Assessment, 1995, 34, 151-162.

14 L. Charerntanyarak, Water Science and Technology, 1999, 39, 135-138.

15 O. E. Abdel Salam, N. A. Reiad and M. M. ElShafei, Journal of Advanced Research, 2011, 2, 297-303.

16 C. Somerfield and N. Hilal, Separation & Purification Reviews, 2011, 40, 209-259.

17 M. Karnib, A. Kabbani, H. Holail and Z. Olama, Energy Procedia, 2014, 50, 113-120.

18 P. N. Dave and L. V. Chopda, Journal of Nanotechnology, 2014, 2014, 14.

19 C. Wang, J. Li, X. Sun, L. Wang and X. Sun, Journal of Environmental Sciences, 2009, 21, 127-136.

20 N. M. Mubarak, J. N. Sahu, E. C. Abdullah and N. S. Jayakumar, Separation & Purification Reviews, 2014, 43, 311-338.

21 C.-H. Zhang, G.-J. Li and J.-H. Wang, Chinese Journal of Analytical Chemistry, 2014, 42, 607-615.

22 M. Mon, J. Ferrando-Soria, T. Grancha, F. R. Fortea-Pérez, J. Gascon, A. Leyva-Pérez, D. Armentano and E. Pardo, Journal of the American Chemical Society, 2016, 138, 7864-7867.

23 Q. Sun, B. Aguila, J. Perman, L. D. Earl, C. W. Abney, Y. Cheng, H. Wei, N. Nguyen, L. Wojtas and S. Ma, Journal of the American Chemical Society, 2017, 139, 2786-2793.

24 A. Chakraborty, S. Bhattacharyya, A. Hazra, A. C. Ghosh and T. K. Maji, Chemical Communications, 2016, 52, 2831-2834.

25 H. B. Bartl and T. Scheller: N. Jb. Miner. Mh, 1970, 35 547–552.

26 J. A. Imlach, L.S.D. Glasser, and P. F. Glasser, *Cement Conc. Res.* 1971, 1, 57–61.

27 S. Watauchi, I. Tanaka, K. Hayashi, M. Hirano and H. Hosono, Journal of Crystal Growth, 2002, 237-239, 801-805.

28 R. W. Nurse, R. W, J. H. Welch & A. J. Majumdar, 1965, Vol. 64.

29 K. Hayashi, M. Hirano and H. Hosono, The Journal of Physical Chemistry B, 2005, 109, 11900-11906.

30 S. Matsuishi, Y. Toda, M. Miyakawa, K. Hayashi, T. Kamiya, M. Hirano, I. Tanaka and H. Hosono, Science, 2003, 301, 626-629.

31 S. W. Kim, S. Matsuishi, T. Nomura, Y. Kubota, M. Takata, K. Hayashi, T. Kamiya, M. Hirano and H. Hosono, Nano Letters, 2007, 7, 1138-1143.

32 M. Miyakawa, H. Kamioka, M. Hirano, T. Kamiya, P. V. Sushko, A. L. Shluger, N. Matsunami and H. Hosono, Physical Review B, 2006, 73, 205108.

33 H. Katsuro, H. Masahiro and H. Hideo, Chemistry Letters, 2005, 34, 586-587.

34 G. Kresse and J. Furthmüller, Physical Review B, 1996, 54, 11169-11186.

35 G. Kresse and D. Joubert, Physical Review B, 1999, 59, 1758-1775.

36 J. P. Perdew, K. Burke and M. Ernzerhof, Physical Review Letters, 1996, 77, 3865-3868.

37 H. J. Monkhorst and J. D. Pack, Physical Review B, 1976, 13, 5188-5192.

38 W. H. Press, S. A. Teukolsky, W. T Vetterling & B. P. Flannery, Numerical recipes in C (2nd ed.): the art of scientific computing. (Cambridge University Press, 1992).

39 S. Grimme, J. Antony, S. Ehrlich and H. Krieg, The Journal of Chemical Physics, 2010, 132, 154104.

40 P. Varotsos, Physical Review B, 2007, 76, 092106.

41 P. Varotsos, Solid State Ionics, 2008, 179, 438-441; A. Chroneos and R. V. Vovk, Solid State Ionics, 271, 1 (2015); V. Saltas, E. N. Sgourou, F. Vallianatos, and A. Chroneos, Appl. Phys. Rev. 4, 041301 (2017).

42 P. V. Sushko, A. L. Shluger, Y. Toda, M. Hirano and H. Hosono, Proceedings of the Royal Society A: Mathematical, Physical and Engineering Sciences, 2011, 467, 2066-2083.

43 F. L. Hirshfeld, Theoretica chimica acta, 1977, 44, 129-138.

44 R. T. Myers, Journal of Chemical Education, 1990, 67, 307.

Table 1. Encapsulation energies (calculated using the metal atom as the reference state) and Bader charges on encapsulated metal atoms in $C12A7:O^{2-}$.

	Heavy metals						
	Cr	Ni	Cu	Zn	Cd	Hg	Pb
Encapsulation energy (eV)	−1.53	−1.69	−1.20	−0.41	−0.16	−0.28	−0.34
Bader charge (|e|)	0.27	0.02	0.004	0.03	0.05	−0.05	0.18

Table 2. Ca-Ca cross cage distance and bond distances between heavy metals and the cage wall ions in relaxed configurations.

	Ca-Ca (Å)	Ca-HM (Å)	Al-HM (Å)	HM-O (Å)
Cr	5.79	2.88	2.99	2.25
Ni	5.71	2.76	2.88, 2.93	2.16
Cu	5.65	2.84	2.78, 2.94	2.17, 2.20
Zn	5.88	2.93, 2.97	—	—
Cd	5.95	2.97, 3.00	—	—
Hg	5.94	2.97, 2.98	—	—
Pb	6.02	3.00	—	2.80

Table 3. Encapsulation energies to add a 2nd and then 3rd heavy metal atom into separate cages in C12A7:O^{2-} . Bader charges are also reported.

Properties	Heavy metal M	M:MC12A7:O^{2-}	M:2MC12A7:O^{2-}
Encapsulation energy (eV/atom) with respect to atom	Cr	–0.45 eV	–1.34 eV
	Ni	–2.57 eV	–1.72 eV
	Cu	–2.70 eV	–1.45 eV
Bader charge |e|	Cr	–0.26, +0.81	+0.25, +0.28, +0.45
	Ni	–0.26, +0.26	–0.29, +0.11, +0.16
	Cu	–0.57, +0.51	–0.57, –0.01, +0.52

Table 4. Encapsulation energies of heavy metal atoms calculated using the metal atom as the reference state and Bader charges on encapsulated metal atoms in $C12A7:e^-$.

	Heavy metals						
	Cr	Ni	Cu	Zn	Cd	Hg	Pb
Encapsulation energy (eV)	−1.94	−3.94	−3.29	−0.66	−0.38	−0.52	−2.38
Bader charge (|e|)	−0.33	−0.98	−0.61	−0.20	−0.14	−0.29	−1.38

Table 5. Cage pole Ca-Ca and Ca-HM distances observed in the relaxed structures.

Atom	Ca-Ca (Å)	Ca-HM (Å)
Cr	5.88	2.94
Ni	5.38	2.69
Cu	5.69	2.85
Zn	5.89	2.94
Cd	5.97	2.99
Hg	5.96	2.98
Pb	5.87	2.93, 2.94

Table 6. Encapsulation energies and Bader charges for the successive encapsulation of Cr, Ni, Cu and Pb in C12A7:e^-.

Properties	Heavy metal atom M	M:MC12A7:e^-	M:2MC12A7:e^-	M:3MC12A7:e^-	M:4MC12A7:e^-
Encapsulation energy(eV/atom)	Cr	−1.76	−1.78	−1.75	−1.18
	Ni	−3.56	−2.92	−1.83	−1.55
	Cu	−3.07	−3.07	−3.02	−1.12
	Pb	−1.48	−0.98	−0.79	−0.47
Bader charge |e|	Cr	−0.33 (2)	−0.31(3)	−0.30 (4)	−0.20 (5)
	Ni	−0.90 (2)	−0.71(3)	−0.55 (4)	−0.42 (2), −0.43 (3)
	Cu	−0.60 (2)	−0.58 (3)	−0.58 (4)	−0.46 (5)
	Pb	−0.78 (2)	−0.51 (2), −0.54	−0.38(4)	−0.26 (3), −0.29 (2)

This manuscript was accepted by J. Appl. Phys. Click here to see the version of record.

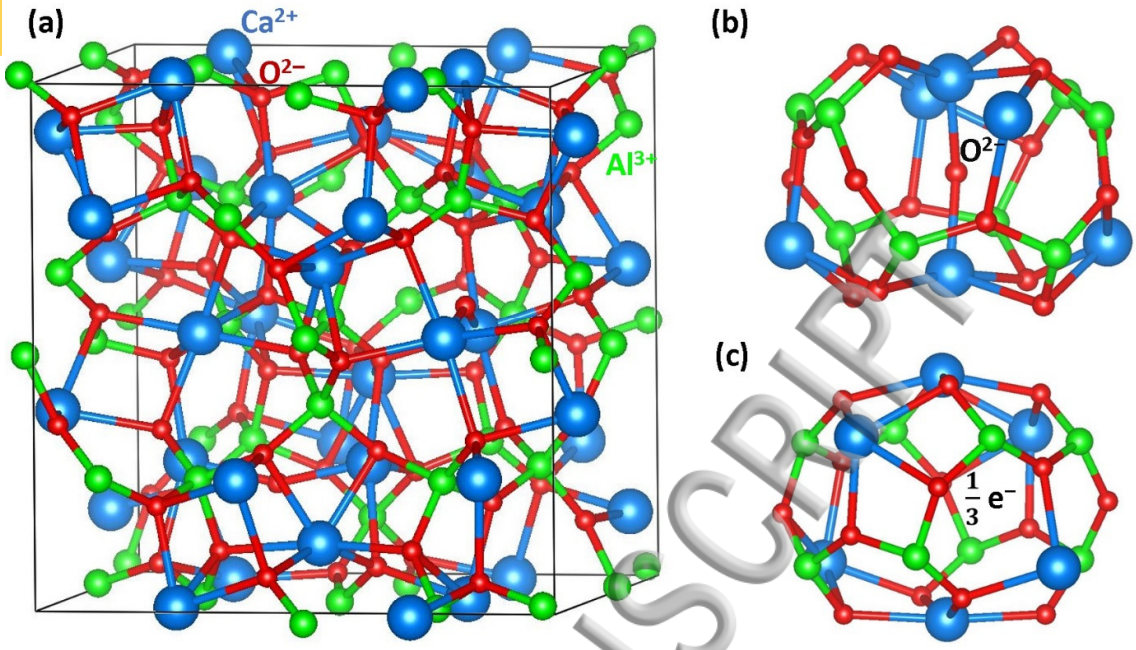

Fig 1 (a) Unit cell framework crystal structure of $[Ca_{24}Al_{28}O_{64}]^{4+}$ with 12 empty cages (EC) **(b)** a relaxed cage containing an extra-framework O^{2-} ion in C12A7:O^{2-} and **(c)** a relaxed cage containing $\frac{1}{3}$ electron in C12A7:e^-.

This manuscript was accepted by J. Appl. Phys. Click here to see the version of record.

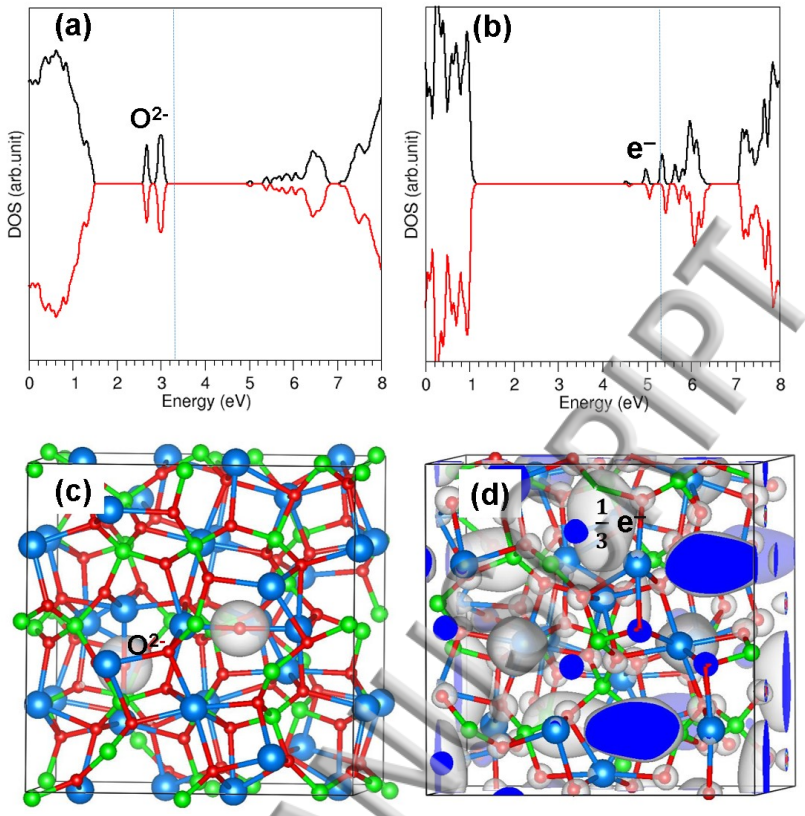

Fig 2 DOS plots for **(a)** C12A7:O^{2-} and (b) C12A7:e^- and surfaces of the constant charge density owing to **(c)** two extra-framework O^{2-}ions in C12A7:O^{2-} and **(d)** four extra-framework electrons in C12A7:e^-.

This manuscript was accepted by J. Appl. Phys. Click here to see the version of record.

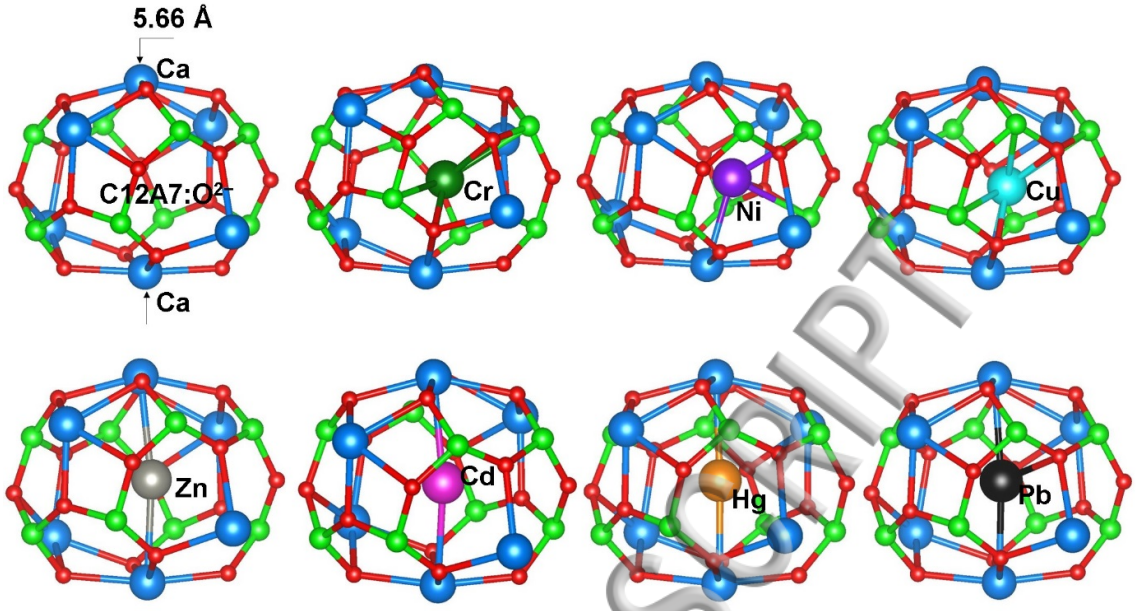

Fig 3 Relaxed structures of heavy metal atom occupied cages of $C12A7:O^{2-}$.

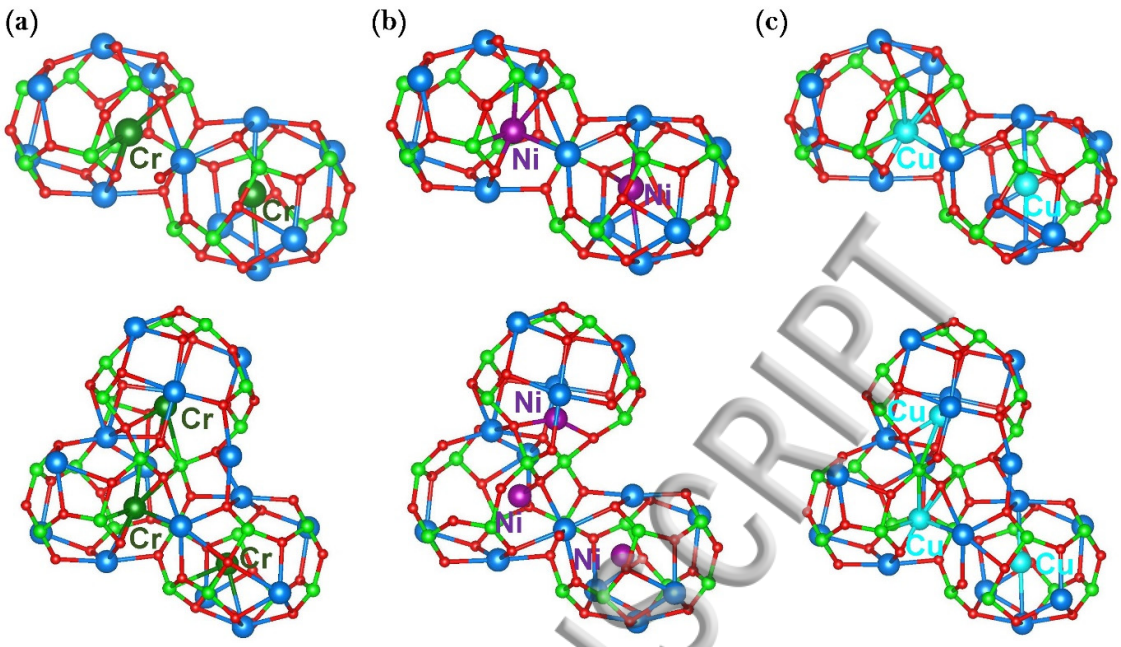

Fig 4 Relaxed cages containing two and three **(a)** Cu **(b)** Ni and **(c)** Cr atoms.

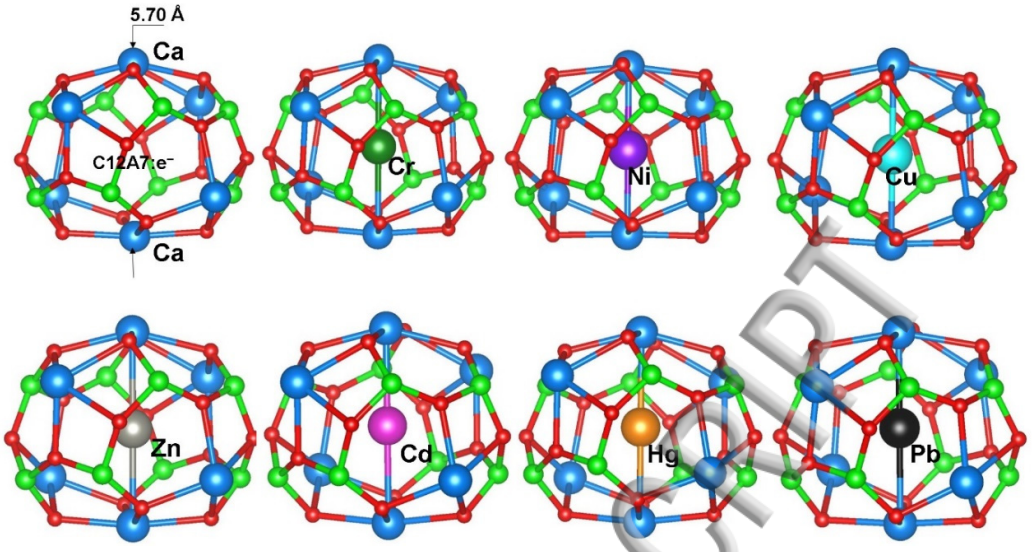

Fig 5 Relaxed structures of heavy metal atoms occupied cages in C12A7:e⁻.

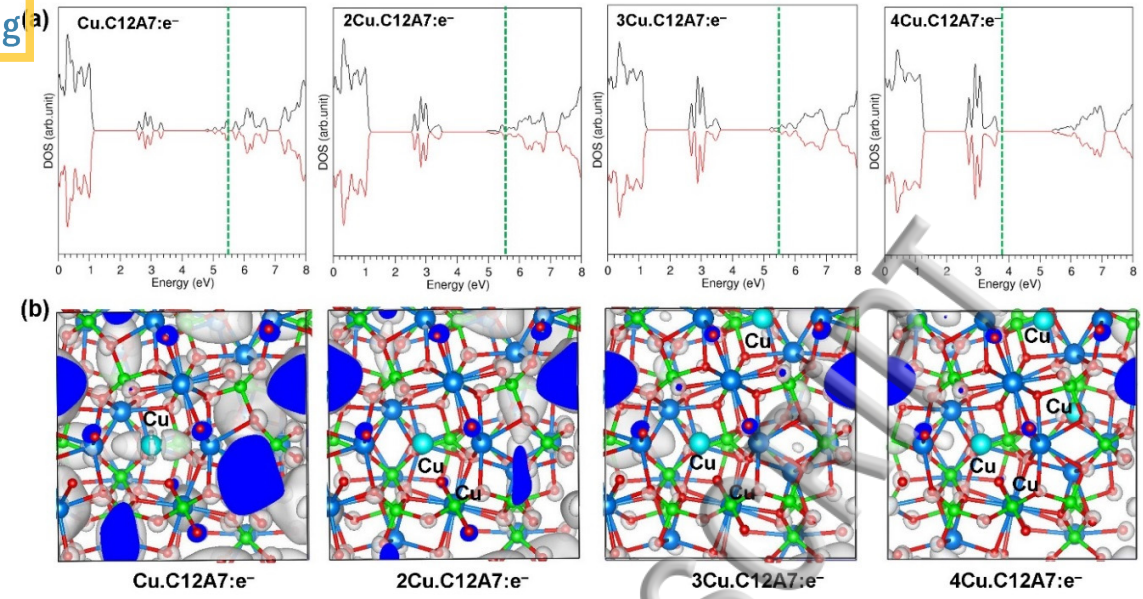

Fig 6 (a) DOS plots for C12A7:e⁻ with respectively Cu, 2Cu, 3Cu and 4Cu encapsulated atoms. The Fermi level is indicated by vertical dotted lines. **(b)** surface of the constant charge density associated with the sates below the Fermi energy.

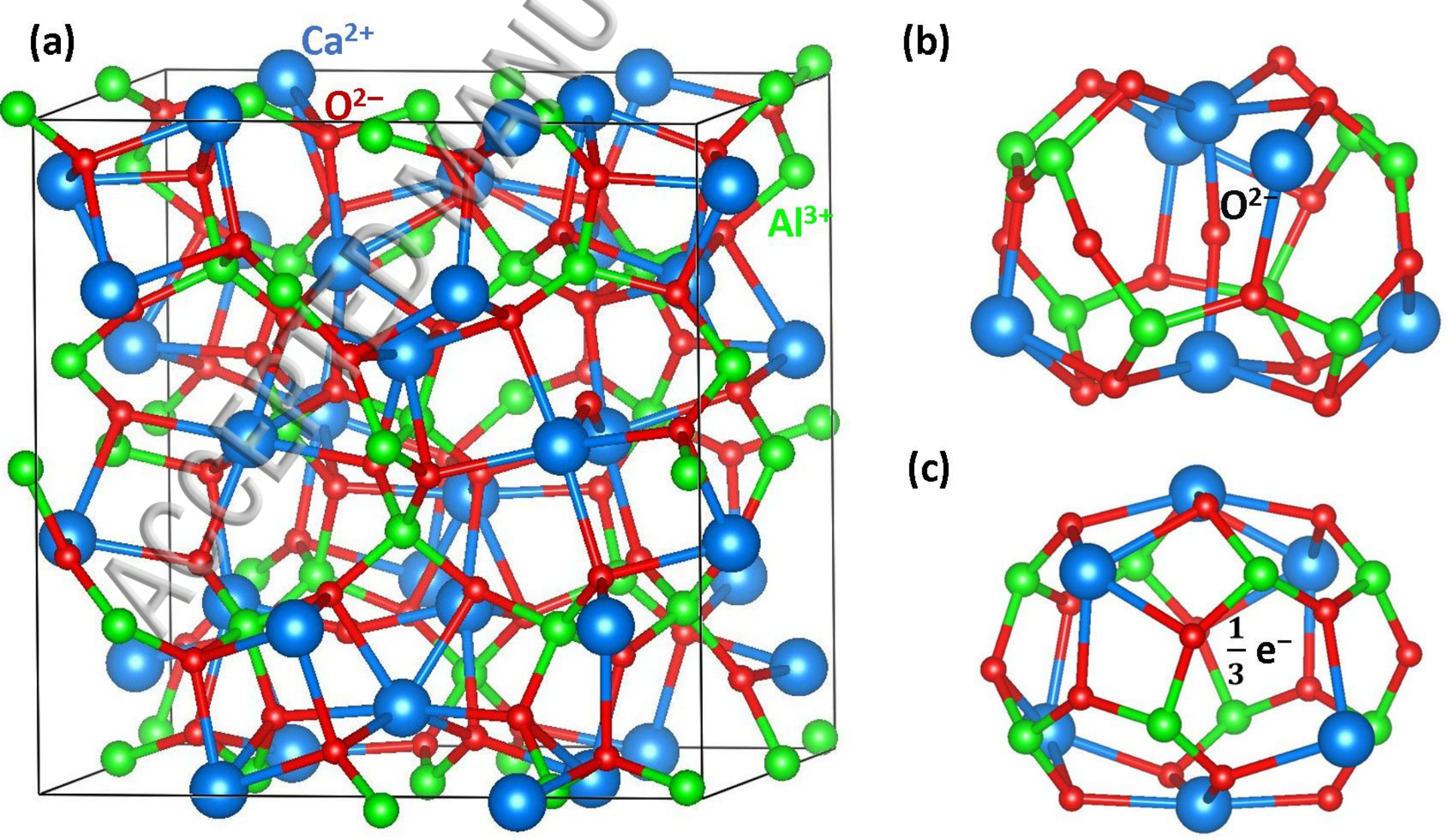

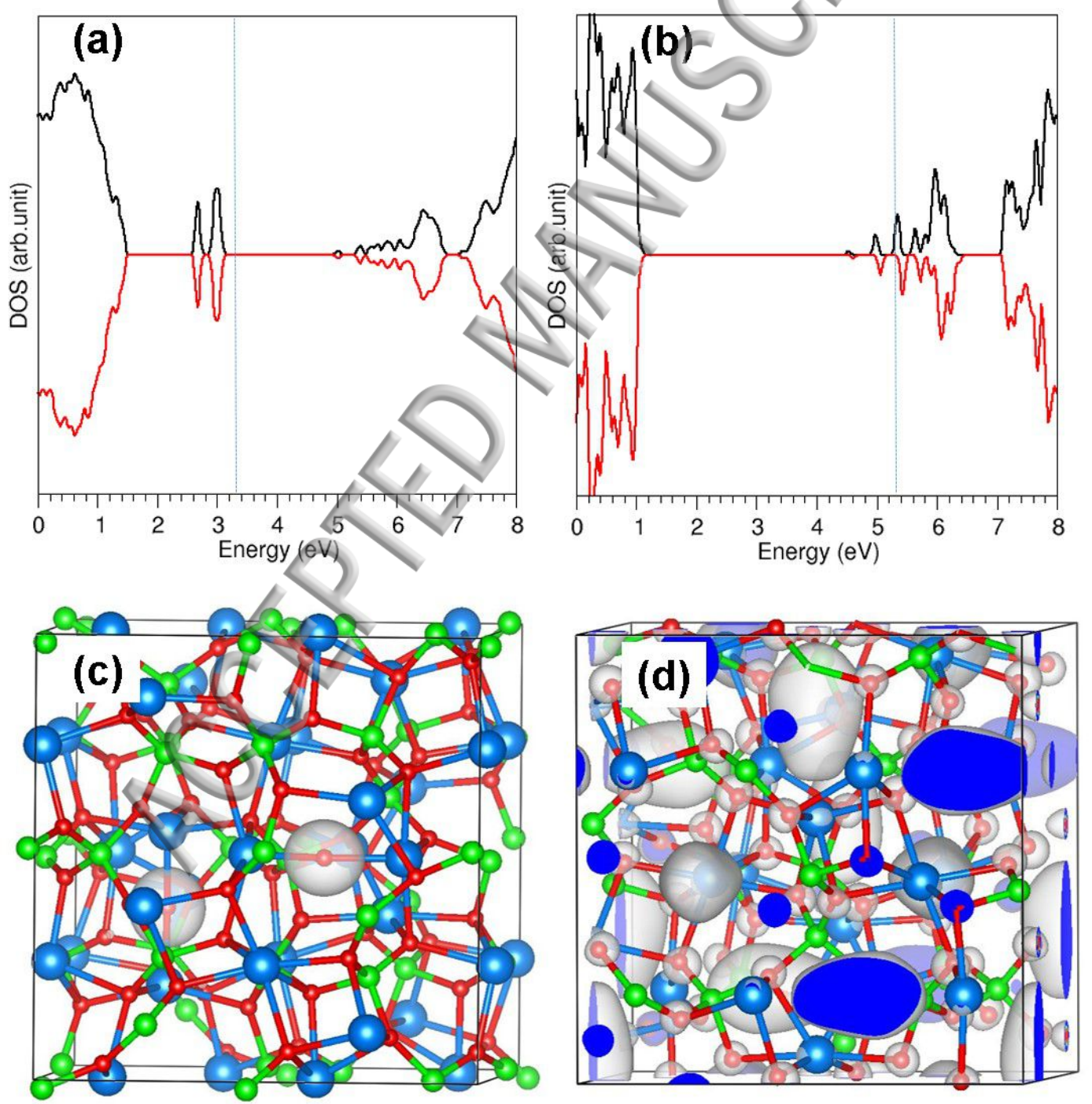

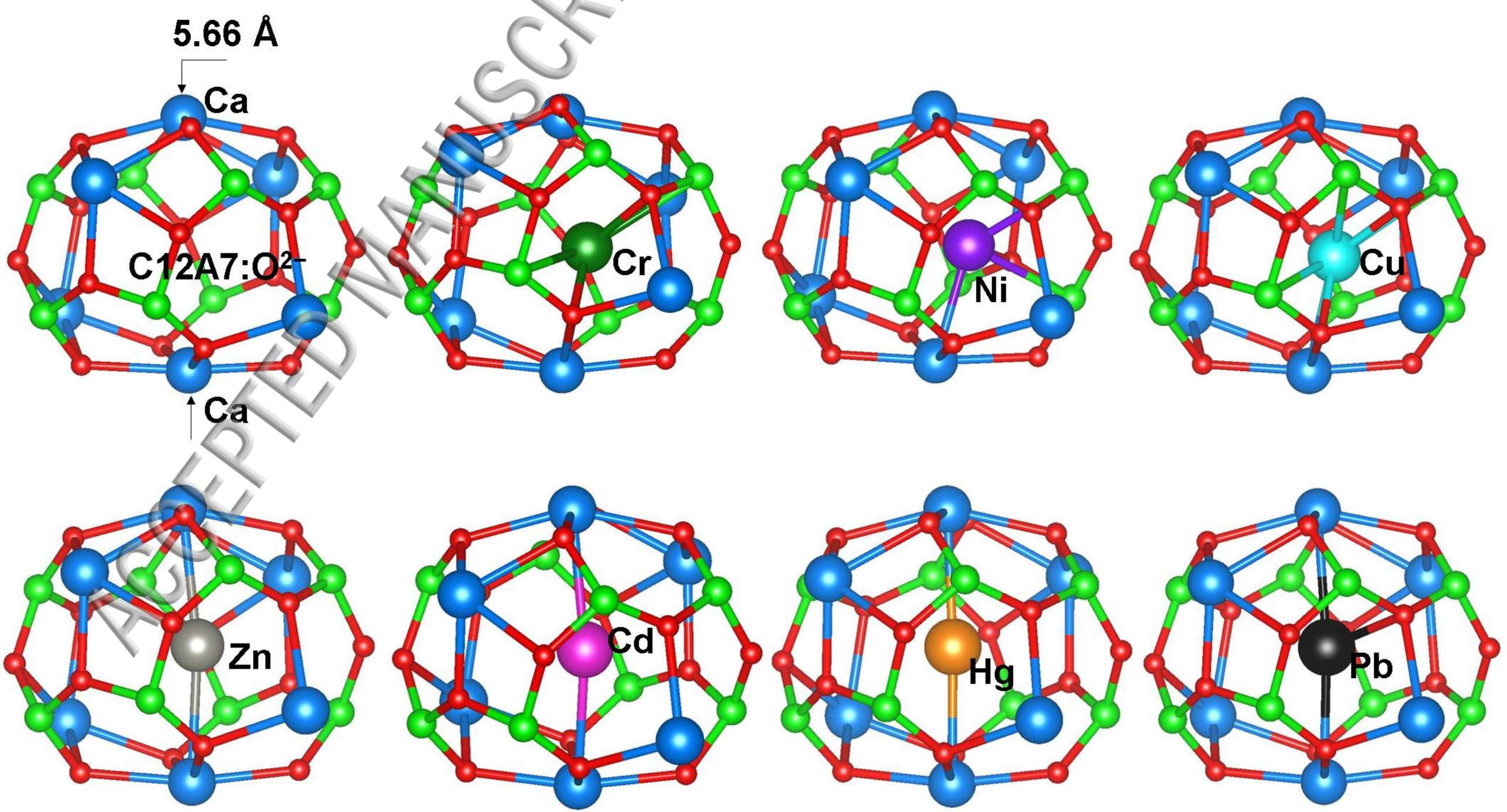

(a)

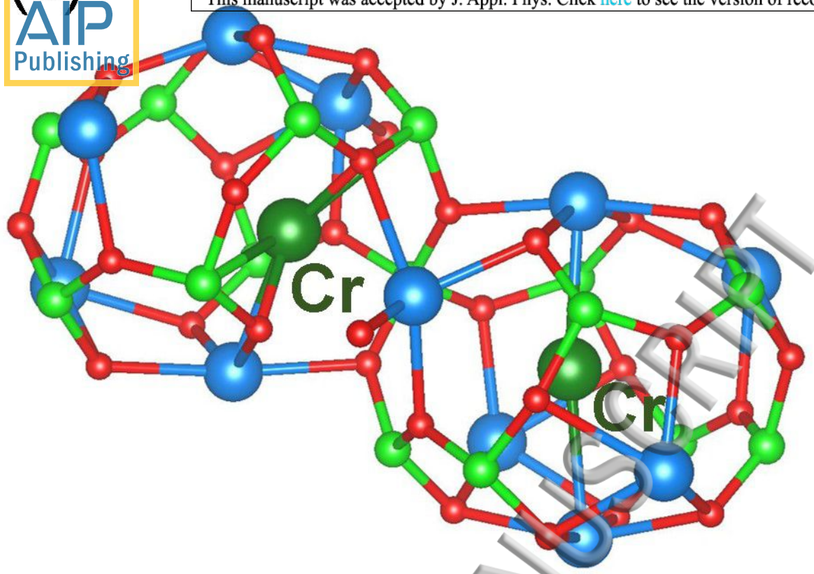

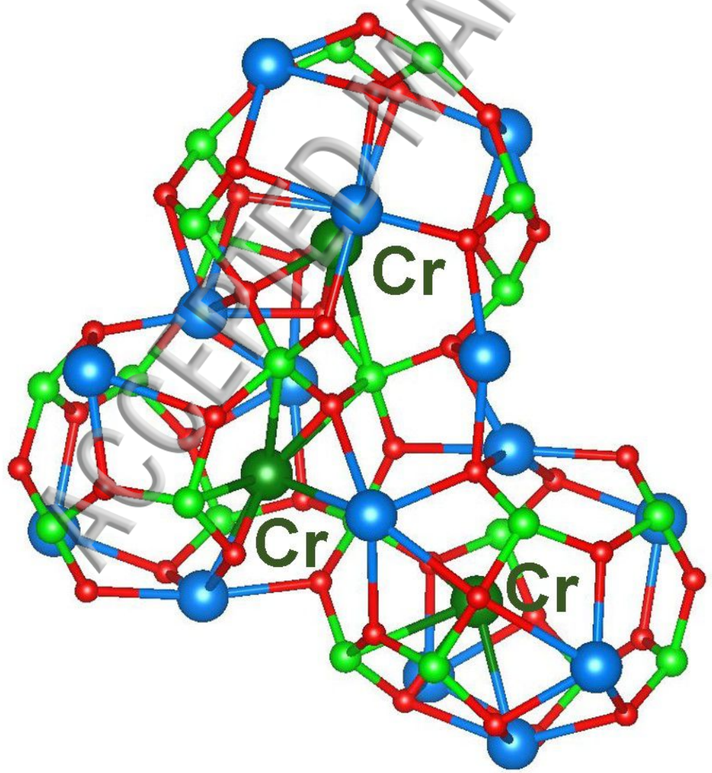

(b)

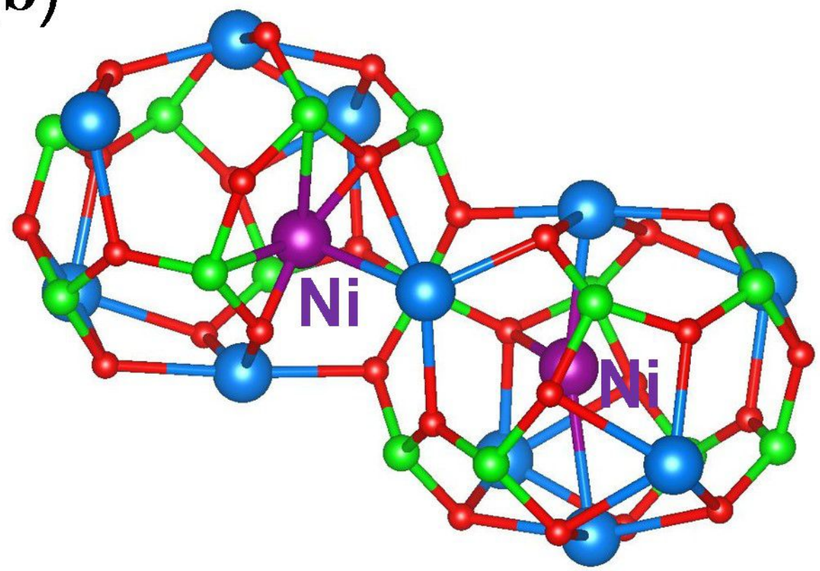

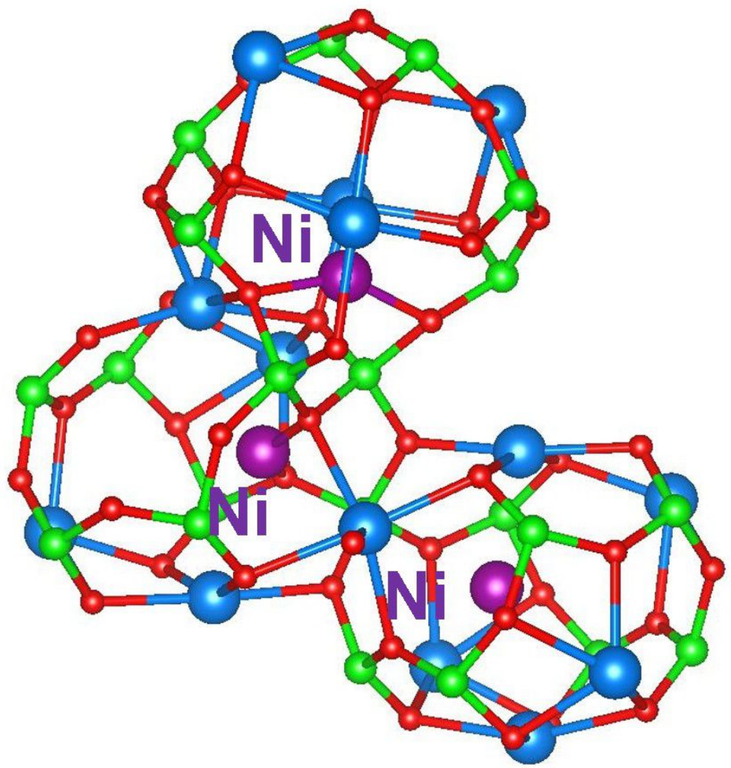

(c)